Lipid Mediator Informatics-Lipidomics: Novel Pathways in Mapping Resolution

Charles N. Serhan,[1] Song Hong,[1] and Yan Lu[1]

[1]Center for Experimental Therapeutics and Reperfusion Injury, Department of Anesthesiology, Perioperative and Pain Medicine, Brigham and Women's Hospital and Harvard Medical School, 75 Francis Street, Boston, MA 02115

ABSTRACT

Lipidomics, the systematic decoding of lipid-based information in biosystems, is composed of identifying and profiling lipids and lipid-derived mediators. As currently practiced, lipidomics can be subdivided into architecture/membrane lipidomics and mediator lipidomics. The mapping of structural components and their relation to cell activation as well as generation of potent lipid mediators and networks involves a mass spectrometry–computational approach so that interrelationships and complex mediator networks important for cell homeostasis can be appreciated. Cell membranes are composed of a bilayer that contains phospholipids, fatty acids, integral membrane proteins, membrane-associated proteins, sphingolipids, and so on. The membrane composition of many cell types has been established. The components' organization and effect on cell function remains to be established, however, and is a quest for lipidomics. Here, we review liquid chromatography tandem mass spectrometry-based lipidomic analyses to address bioactive lipid mediators in signaling pathways and the roles of lipid-derived mediators in resolution of inflammation.

INTRODUCTION

Given swift advances in genomics and proteomics, it appears that metabolomics (Figure 1A)—that is, the appreciation of metabolic networks and pathway intermediates—is the next step in our molecular appreciation of the basis of life (from gene to functioning organism). The structure-activity relationships for bioactive lipids conceptually antecede the current appreciation of biological mass spectrometry (MS) as well as so-called chemical biology and genetics. Initial studies showed that prostaglandins are potent fatty acid–derived local-acting mediators (Figure 1B) important in a wide range of processes, such as inflammation, labor, hemodynamics, and renal function.[1,2] These studies are reminders of the importance of identifying and profiling compounds and their further metabolites by mass spectral–based methods. Gas chromatography and corresponding MS methods are well established and useful in probing bioactive lipid mediators (LMs).[2] Advances in computer hardware, software, algorithms, chromatography, and identification of bioactive mediators help to establish our appreciation for what is currently termed *mediator lipidomics* or *mediator profiling* (Figure 2).[3,4] Advances in the use of liquid chromatography tandem mass spectrometry (LC-MS/MS) permit profiling of closely related compounds without requiring derivatization of samples. Moreover, the interface of MS/MS with LC permits profiling of LMs with reduced potential for workup-induced artifacts. This review outlines our recent studies and uses of mediator lipidomics in biomedical systems of interest.

DIVERSITY OF LIPID STRUCTURES AND SCOPE OF LIPIDOMICS

Cell membranes are composed of a phospholipid bilayer, which is depicted in Figure 1A as being split down its hydrophobic region; the bilayer illustration shows a sea of phospholipids and was created with results from freeze-etched electron micrograms. The membranes' organization and the precise composition of microdomains surrounding key integral membrane proteins, subcellular membranes, and other lipid-enriched domains within cells have yet to be appreciated in detail. We have only limited information on the organization of and interactions within discrete lipid patches, also known as microdomains, and on how they affect the function of cell membranes. Nonetheless, these microdomains, including lipid rafts, are of considerable interest for their role in regulating signal transduction. Identifying the 3 major phospholipids (phosphatidic acid, phosphatidyl choline, and phosphatidyl ethanolamine), their major phosphate linkage groups, and their fatty acids (myristic acid, palmitic

Corresponding Author: Charles N. Serhan, Director, Center for Experimental Therapeutics and Reperfusion Injury, Thorn Building for Medical Research, 7th Floor, Brigham and Women's Hospital, Boston, MA 02115. Tel: (617) 732-8822; Fax: (617) 582-6141; E-mail: cnserhan@zeus.bwh.harvard.edu
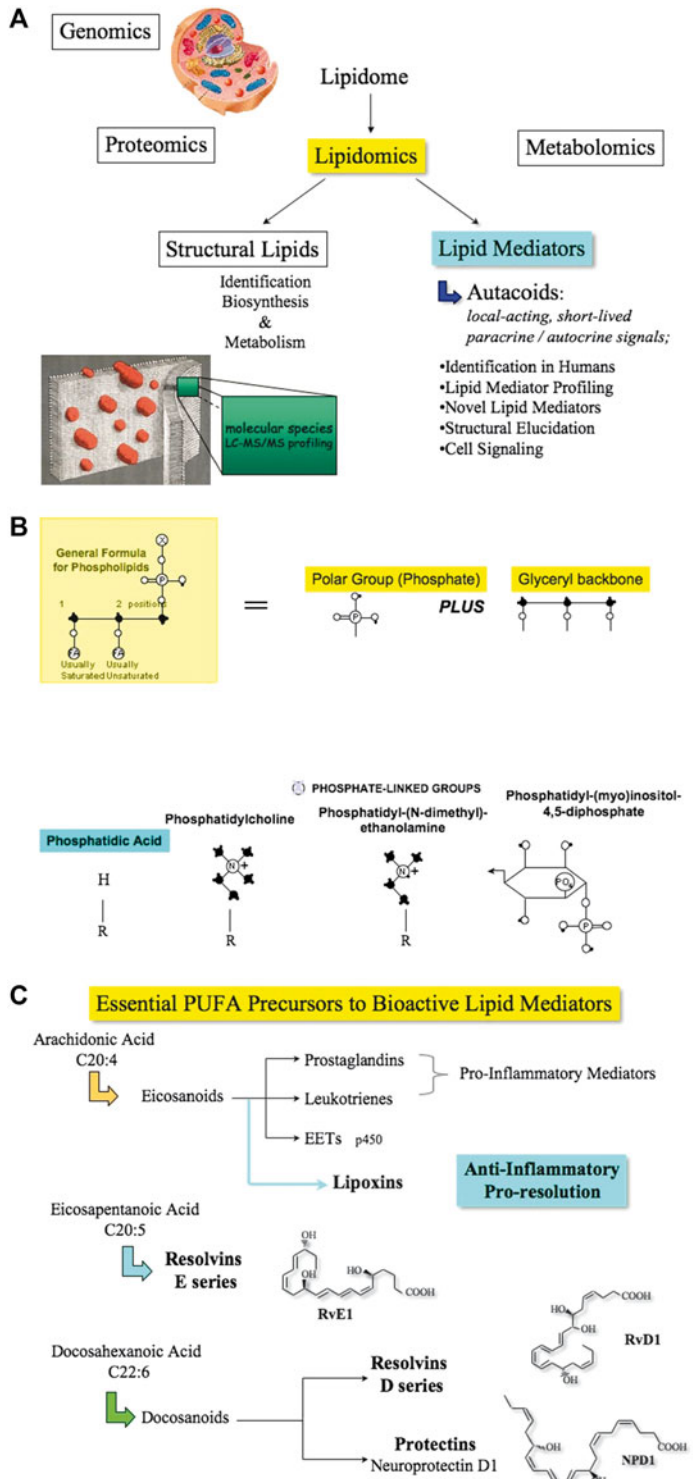
acid, steric acid, oleic acid, linoleic acid, linolenic acid, and arachidonic acid, each named by its increasing carbon chain length and degree of unsaturation, ie, double bonds and their position) (Figure 1B) is challenging. Each phospholipid contains 2 fatty acids in the 1 and 2 positions that establish the complete identity and coordinates of each individual phospholipid. Moreover, the phospholipid physical properties are governed by a different acyl chain composition that can have a dramatic impact on cell function.

Sphingolipids are another form of complex lipid that can also give rise to signaling molecules.[5] Sphingosines are made of phosphate and choline, such as sphingomyelin, and are well appreciated for their ability to insulate neurons and ceramide, cerebroside, and ganglioside groups. The chemical composition and biosynthesis of each of the major classes of sphingosine structures is known. However, how sphingosines are organized within membrane structures and their dynamics during cell activation and generation of intracellular second messengers have yet to be fully appreciated. Understanding these fatty acid acyl chains and their organization for each lipid species is a quest for lipidomics. One research group focusing on these and related sphingolipid compounds using a lipidomics approach is at the Medical University of South Carolina (http://hcc.musc.edu/research/shared_resources/lipidomics.cfm). The National Institute of General Medical Sciences (NIGMS) Lipid Metabolites and Pathways Strategy (MAPS) consortium is currently studying triglyceride structure and the function of phosphatidylinositol and other sugar-linked phospholipids in cell signaling (see http://www.nigms.nih.gov/funding/gluegrants.html and http://www.lipidmaps.org). A goal of this consortium is to assemble maps of key lipids, that is, phospholipids and lipid-derived mediators.

LIPID SIGNALS AND AUTOCOIDS

Diacylglycerol (DAG) is an intracellular second messenger that helps to illustrate the potential for second messenger lipidomics. We recently linked a genetic abnormality in patients with local aggressive periodontal disease to impaired DAG kinase activity in their peripheral blood neutrophils. This familial disorder is characterized by supporting structures of the dentition.[6] In these patients, white

Figure 1. Scope of the problem for mediator lipidomics within the lipidome. (A) Structural lipids and lipid mediators. (B) the major phospholipid subunits on a glycerol framework addition of specific polar groups and fatty acids in the 1 or 2 position constituting specific phospholipid classes. For example, phosphatidic acid can represent multiple molecular species given the many different fatty acids possible in its number 1 or 2 position (1 and 2 position is distinctly different from the properties of 1 position and arachidonic acid). Each of these individual molecular species (>1000 distinct molecules) gives rise to unique physical properties such as different molecular ions, retention times, and fragmentation on LC-MS/MS (liquid chromatography-tandem mass spectrometry) profile analysis. (C) families of bioactive lipid autocoids. Arachidonic acid is the precursor for many of the known bioactive mediators, EETs (epoxyeicosatrienoic acid), prostaglandins, leukotrienes, and lipoxins (both pro- and antiinflammatory mediators). The omega-3 PUFAs, EPA (eicosapentaenoic acid) (C22:5) and DHA (docosahexaenoic acid) (C22:6), are precursors to potent new families of mediators termed resolvins and protectins.
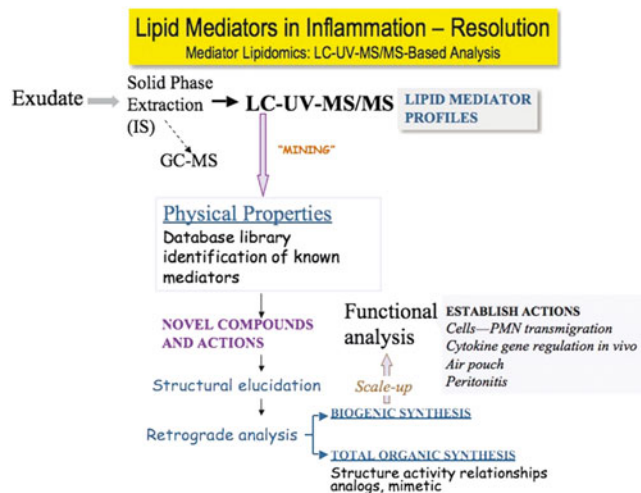
Figure 2. Mediator lipidomics via LC-UV-MS/MS (liquid chromatography-ultra violet and tandem mass spectrometry) analysis of the physicochemical properties including tandem mass and UV spectra and chromatographic profiles.

blood cells, specifically neutrophils, the first line of defense to host infection, display reduced chemotaxis toward microbes. Neutrophils from these patients show reduced transmigration and decreased ability to generate reactive oxygen species. Using a lipidomics approach to identify molecular species at positions in the 1,2 diacyl-sn-3-glycerol backbone in these patients' neutrophils, we found alterations in levels and specific molecular species.[6] LC-MS/MS-based lipidomics was performed to identify and quantitate relative amounts of individual species of DAGs involved in second messenger signaling. Profiles of specific DAG species were identified by their physical properties, including molecular ions and specific daughter ions, and by coelution with authentic standards of the major species. We demonstrated both molecular and temporal differences in DAG signaling species between (1) white blood cells (neutrophils) obtained from healthy individuals, and (2) neutrophils from patients with localized aggressive periodontal disease.[6] Hence, this type of structure-function profiling of intracellular messengers improves our appreciation of signaling pathways and their alterations in disease.

METABOLOMICS AND MEDIATOR LIPIDOMICS IN ENGINEERED EXPERIMENTAL ANIMALS

Another powerful use of mediator lipidomics can be illustrated by studies with transgenic animals (eg, transgenic rabbits).[7] In general, unsaturated double bonds present in polyunsaturated fatty acids (PUFA), such as arachidonic acids, are nonconjugated, making the fatty acids essentially devoid of a characteristic UV spectrum. During the release of arachidonic acid and its transformation to bioactive lipids, specific stereoselective hydrogen abstraction leads to

formation of conjugated diene-, triene-, or tetraene-containing chromophores, particularly in linear eicosanoid groups of mediators, such as the lipoxygenase pathway products leukotrienes (LT) and lipoxins (LX) (Figure 1C). The presence of both specific UV chromophore and characteristic MS/MS spectra, the fragmentation of these compounds, and retention time, together with bioactions, which are usually in the nano- to picomolar range for eicosanoids, display profound stereoselectivity. In general, eicosanoids are rapidly formed within seconds to minutes, act on cells locally, and then are rapidly inactivated. Eicosanoids usually act as extracellular mediators within their local milieu and therefore are grouped in some cases with the broader group of autocoids (eg, serotonin, histamine).

The physical and biological properties of each of these related structures permit identification and profiling from the complex cellular milieu. Unlike phospholipids or other structural lipids, which have a barrier function, those lipid mediators derived from arachidonic acid (eg, prostaglandins, LT, LX) have potent stereoselective actions on neighboring cells (Figure 1A). This makes it very important for profiling efforts to clearly separate these related structures for their identification, since in some cases closely related structures are devoid of bioactions. Hence, accurate profiling and identification of relationships between products within a snapshot of a biological process or disease state can give valuable information.[8] Moreover, when specific drugs are taken, such as aspirin, the relationship between individual pathway products can be changed and their relationship may be directly linked to the drug's action in vivo.[4,9] Hence, mediator lipidomics provides a valuable means to assess the phenotype in many prevalent diseases, particularly those in which inflammation has an important pathologic basis.

The powerful approach of transgenics, namely deletion and/or overexpression of a gene product coupled with lipidomics, can give valuable information and an unbiased assessment of pathways and their interactions in vivo. Recently, we used this LM informatics-lipidomics approach to evaluate transgenic rabbits overexpressing the human 15-lipoxygenase (LOX) type 1 in their leukocytes.[7] When these rabbits' profiles were compared directly to nontransgenic rabbits, in which the key enzyme is not overproduced but is in its normal state; a snapshot can be taken upon cell activation, and the difference between the non-transgenic versus overexpression of the key enzyme in a pathway can be examined. In this example, human 15-LOX overexpression gave enhanced lipoxin A_4, as well as enhanced 5S,15S-dihydroxyeicosatetraenoic acid (5S,15S-diHETE) formation with an apparent reduction in leukotriene B_4 formation. Because leukotriene B_4 is a potent chemoattractant and lipoxin A_4 is a counterregulatory antiinflammatory from the eicosanoid family, their interrelationship(s) and overproduction of lipoxin A_4 are key indices in appreciating the

in vivo role of 15-LOX type 1 in inflammation. Thus, over-expression of 15-LOX type 1 leads to upregulation of its potent bioactive pathway product, namely lipoxin A_4, in these transgenic rabbits that display overall reduced inflammation and protection from tissue damage.

NOVEL LM PATHWAYS IN RESOLUTION

It is now understood that inflammation plays a key role in many prevalent diseases. In addition to the chronic inflammatory diseases, such as arthritis, psoriasis, and periodontitis, as noted above, diseases such as asthma, Alzheimer's disease, and even cancer have an inflammatory component. Therefore, it is important for us to acquire more detailed information on the molecules and mechanisms controlling inflammation[10] and its resolution. Toward this, we recently identified new families of LMs generated from fatty acids during resolution of inflammation, termed *resolvins* and *protectins*.[11,12]

Using systematic analysis, we sampled inflammatory exudates during resolution as leukocytic infiltrates were declining to determine whether there were, indeed, new mediators generated. We used a *functional mediator lipidomics* approach employing LC-MS/MS to evaluate and profile temporal production of compounds (see Figure 2 outline) at defined points during experimental inflammation and its resolution. The focus was on bioactions of potential novel mediators. We constructed libraries of physical properties for known mediators, that is, prostaglandins, epoxyeicosatetraenoic acids, leukotrienes, and LX (see below), as well as theoretical compounds and their potential diagnostic fragments, as signatures for specific enzymatic pathways. When novel compounds were pinpointed within chromatographic profiles, we performed complete structural elucidation as well as retrograde chemical analyses that involved both biogenic and total organic synthesis, which permitted scaling up of the compounds of interest and their evaluation in vitro and in vivo. The in vivo models included a murine air pouch model of inflammation as well as peritonitis. In vitro cell assays focused on regulation of cytokines and leukocyte migration across transepithelial and/or transendothelial monolayers.

Mediator-lipidomic databases containing MS/MS as well as UV spectra and chromatographic profiles with appropriate search algorithms are imperative for accurate and timely analysis of LMs (Figure 2).[3] Although gas chromatography-mass spectrometry (GC-MS) can be used in many cases for identification of structures, the required high column temperatures limit its use because many of the PUFA-derived LMs are thermo-labile.[13] In this context, search algorithms for GC-MS electron-impact-ionization spectra have been well studied,[14-16] as have those for both GC-MS chromatograms and mass spectra.[17] The contrast angle (or dot prod-

uct, the cosine of the contrast angle) algorithm is widely used. The contrast angle is the angle between 2 spectra represented as vectors composed of ordered peak intensities.[16] Since databases and search algorithms for LMs on comprehensive LC-UV-MS/MS are not yet available, we initially used MassFrontier (ThermoFinnigan), GC-MS mass spectral commercial software, to construct an LM database and search algorithm. The search algorithm for MassFrontier is dot product, developed by Stein and Scott.[15,16]

The dot product algorithm in MassFrontier uses the intensities of all peaks in MS/MS as a vector for computation and is not concerned with the identities of ions, whether they are molecular ions, ions derived from molecular ions, or ions from interfering substances in the samples.[14-17] Using the ions generated from interfering background can decrease the percent correct for best match of the search. Even the ions generated from unknown LMs contribute differently to the identification. For LMs, ions generated by cleavage of the carbon-carbon bond inside the carbon chain have greater diagnostic yield for determining the structures than the ions formed by loss of water or CO_2. Ions formed by loss of water or CO_2 are common in most PUFA-derived LMs.[9,13,18-20]

Relationships between electrospray tandem mass spectrometry (ESI-MS/MS) spectra and LM structures have been studied extensively and are well understood.[4,9,13,19-21] The identification and elucidation of the unknown structures of novel LMs by LC-UV-MS/MS is based on the relationships between structural features (eg, functional groups, double bonds) and characteristics of the spectra and chromatograms (MS/MS ions, UV spectra, and LC retention times). On C18 reversed-phase LC, chromatographic retention times (CRTs) generally increase in the following order: trihydroxy-containing LMs, dihydroxy-containing LMs, and monohydroxy-containing LMs. Then the nonoxidized PUFA precursors (eg, arachidonic acid) are eluted, depending on the mobile phase employed. For positional isomers of hydroxy-containing LMs, the CRTs decrease as the hydroxy groups locate closer to the methyl group at the omega end of the long-chain PUFA. For instance, the CRT of LXB_4 ($5S,14R,15S$-trihydroxy-$6E,8Z,10E,12E$-eicosatetraenoic acid) is usually shorter than that of LXA_4 ($5S,6R,15S$-trihydroxy-$7E,9E,11Z,13E$-*trans*-11-*cis*-eicosatetraenoic acid). The CRT of native LXA_4 (containing a 15S-hydroxy at carbon 15) is shorter than that of the aspirin-triggered 15-epi-LXA_4 but greater than that of 11-*trans*-LXA_4, which is the natural all-*trans*-containing isomer of LXA_4.[22]

The UV spectrum, namely the band multiplicity and λ_{max}, are additional signatures of specific LMs. For example, the presence of an asymmetric singlet band with λ_{max} ~235 nm for the conjugated diene present within the lipoxygenase pathway represents the mono-OH compounds. These include mono-HETEs (mono-hydroxy-eicosatetraenoic acids); a triplet

with λ_{max} ~270 nm for the leukotrienes such as the conjugated triene within LTB$_4$ (5S,12R-dihydroxy-6E,8Z,10Z,14E-eicosatetraenoic acid); and a triplet with λ_{max} ~300 nm for conjugated tetraene as present within LXA$_4$ and LXB$_4$. Another example would be an asymmetric singlet with λ_{max} ~242 nm from the 2 conjugated dienes interrupted by a methylene group as present in the double lipoxygenation product 5S,15S-diHETE.[22] Some compounds of interest do not possess specific chromophores, namely diene-, triene- or tetraene-containing conjugated systems. For example, those with λ_{max} in vacuum UV range (actually undetectable on the currently used LC-UV-MS/MS) as 1,4-cis-pentadiene containing PUFA, and some prostaglandins such as PGE$_2$ (11α,15S-dihydroxy-9-oxo-prosta-5Z,13E-dien-1-oic acid) and PGF$_{2\alpha}$ (9α,11α,15S-trihydroxy-prosta-5Z,13E-dien-1-oic acid), that do not possess conjugated double-bond systems.[22,23] When the conjugated tetraene of LXA$_4$ isomers is in the all-*trans*-geometry, the λ_{max} is shifted to 302 nm instead of 300 nm.[22] The relationships between MS/MS spectra and LM structures are of interest and presented below.

Using current chemical analytical technologies, most LMs are identified manually by comparing the spectra and chromatographic behaviors acquired from sample tissues with those of authentic standards of known LMs. When authentic standards are not available, as in the case of novel LMs and their further metabolites, basic chemical structures can be obtained on the basis of the relationship between structures and features of their spectra and chromatographic behaviors are compared with those of synthetic and biogenic products prepared to assist in the assignment. We routinely identify LMs by matching the unknown spectra (MS/MS, GC-MS, and UV spectra) and CRTs to those of authentic and synthetic standards if available, or with a theoretical database that consists of virtual UV and MS/MS spectra and CRTs for discovering potentially novel LMs[3,9,20] if standards are not available. We initially developed a theoretical database and algorithm according to the relationships between LM structures and their spectral and chromatographic characteristics.[3] The proposed structures of novel potential LMs in the theoretical databases were based on PUFA precursors and established biosynthetic pathways.

We constructed mediator-lipidomic databases and search algorithms to assist in the identification of LM structures employing LC-UV-ion trap MS/MS with the following objectives: (1) assembling a database using currently available mass spectral software; (2) constructing a cognoscitive-contrast-angle algorithm and databases to improve the identification of LMs using MS/MS ion identities that currently cannot be performed with available software; and (3) developing a theoretical database and algorithm for assessing potentially novel and/or unknown structures of LMs and their further metabolites in biologic matrices. It is quite

meaningful to develop mediator-lipidomic databases and algorithms using ion trap mass spectrometers, because they are relatively inexpensive instruments that are widely used. Moreover, the fragmentation rules and patterns for collision-induced dissociation (CID) spectra from triple-quadruple mass spectrometers, another popular type of MS instrumentation, are similar to what we encounter using ion trap mass spectrometers.[7,13,24]

LOGIC DIAGRAM TO IDENTIFY LMs: LIPIDOMIC DATABASES AND ALGORITHMS

The regular routes for LM identification and structure elucidation of potentially novel LMs were followed in mediator-lipidomic databases and search algorithms that we constructed (Figure 3). Two types of lipidomic databases for LMs were used for searching: one contains LC-UV-MS/MS spectra and chromatograms acquired on LM standards, and the other is based on theoretically generated LC-UV-MS/MS spectra and chromatograms. The searches were conducted stepwise against either standards or the theoretical databases to increase the search speed. The search of MS/MS spectra was performed against only the MS/MS subdatabase with the molecular ion of interest (ie, M-1) and matched UV spectra (eg, conjugated diene, triene, or tetraene chromophores). Subsequently, the matching of CRTs was performed. The standard error for CRTs for the chromatographic conditions used in the present set of experiments was ~0.3 minutes. Thus, only the unknown CRT within ±2 × 0.3 minutes of the CRT (for 95% confidence intervals) in the databases was taken as a correct match. If the UV spectral pattern was unclear, the MS/MS and CRT were still searched to avoid potential errors in assignment. A standard LM or theoretical

Logic diagram for developing LC-UV-MS/MS-based mediator lipidomic databases and search algorithms for PUFA-derived LMs.
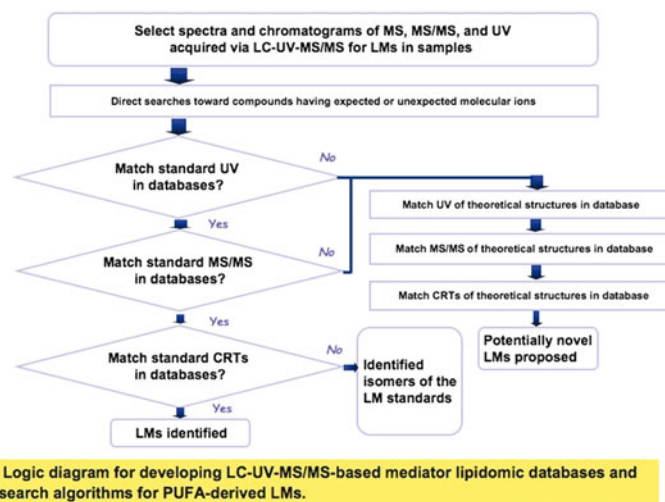
Figure 3. Logic diagram for developing LC-UV-MS/MS (liquid chromatography-ultra violet and tandem mass spectrometry)-based mediator lipidomic databases and search algorithms for PUFA-derived LMs (lipid mediators).

fragmentation/ion fragmentation pattern that fulfilled the above match criteria was then assigned to the unknown set. If the match was a "hit" with UV and MS/MS spectra but not with CRT, the LM in the sample was likely to be a geometric isomer of a known LM.

UV patterns are simply presented in the database as maximum absorbance wavelength λ_{max} and divided into 6 clusters: ~301 nm, ~278 nm, ~270 nm, ~242 nm, ~235 nm, and vacuum UV. In contrast, each MS/MS spectrum has dozens of ions and therefore is a much larger data set than a UV λ_{max}. If the UV λ_{max} is matched first, then only the MS/MS subdatabase having LM standards with this UV λ_{max}, which is a fraction of the whole MS/MS database, needs to be searched. This type of narrowed search is faster than a search through the entire MS/MS database. The reduction in speed will become even more significant when more and more standard MS/MS data are entered into the database. We tested the route with MS/MS spectra before UV; the search results are the same as with MS/MS after UV data. If the UV pattern is unclear, we can search the MS/MS and CRT to avoid potential assignment errors.

DATABASES CONSTRUCTED WITH MASS SPECTRAL SOFTWARE

An LM informatics database composed of LC-UV-MS/MS spectra and chromatograms acquired from authentic LMs was constructed with the GC-MS spectral software Mass-Frontier. The UV λ_{max} of authentic LMs was written into the subdatabase names, and the CRTs were written into the LM names so that MassFrontier could handle the acquired UV spectral results and CRTs for the identification of the unknown LMs following the logic diagram in Figure 3.

The efficacy of this database was assessed with the identification of eicosanoids biosynthesized by rabbit leukocytes using LC-UV-MS/MS (Figure 4). For peak I in the left inset of Figure 4A, a subdatabase mTOz 351Vacuum UV was selected with the molecular ion of interest and matched UV λ_{max}. The search showed that the MS/MS spectrum of peak I matched best with PGE$_2$, with the highest matching score, that is, 907 (Figure 4B). Furthermore, the CRT of peak I and standard PGE$_2$ matched. Therefore, peak I was assigned as PGE$_2$, consistent with the manual identification and assessment of MS and UV spectral and LC chromatographic features of PGE$_2$.

COGNOSCITIVE-CONTRAST-ANGLE ALGORITHM AND DATABASES

Identification of Mass Spectral Ions Generated From LMs

The cognoscitive-contrast-angle algorithm and databases (COCAD) system that we developed (see Levy et al[8]) can
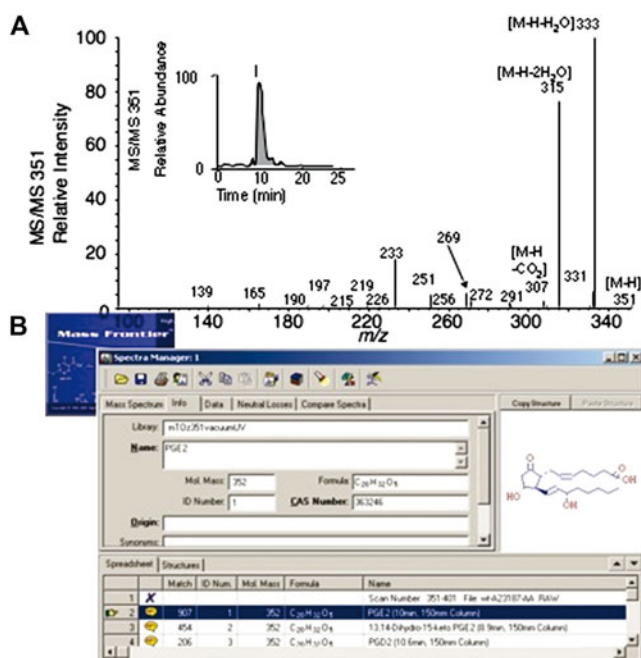

Figure 4. Identification of PGE$_2$ (11α,15S-dihydroxy-9-oxo-prosta-5Z,13E-dien-1-oic acid) generated by rabbit leukocytes using a mediator-lipidomic database and algorithm developed with MassFrontier. (A) MS/MS spectrum and MS/MS of ion mass/charge (m/z) 351 chromatogram (inset) were acquired for PGE$_2$ generated from incubation of rabbit polymorphonuclear neutrophils (PMN) and arachidonic acid (representative, n = 3). The MS/MS scan conditions were parent ion, m/z 351; isolation width, 1.6; normalized collision energy, 42%; activation time, 30 ms; and scan of MS/MS ions, m/z 95 to 355. The liquid chromatography (LC) column used was 150 mm long, with a 2-mm inner diameter, and packed with 5 μm of C-18 particles. The gradient for the mobile phase is detailed in Lu et al.[3] (B) Report for the search via the MassFrontier system indicating PGE$_2$ as the best match.

be used to elucidate the fragmentation of LMs in MS and to match unknown MS/MS spectra to those of synthetic and/or authentic standards. In this matching process, the intensity of each peak is treated differently based on the ion identity. MS/MS ions are clustered into 3 types: peripheral-cut ions, formed by neutral loss of water, CO$_2$, amino acid, or amines derived from functional groups linking to the LM carbon chain as hydroxy, hydroperoxy, carbonyl, epoxy, carboxy, amino acid group, amino group, and so on; chain-cut ions, formed by cleavage of a carbon-carbon bond along the LM carbon chain; and chain-plus-peripheral-cut ions, formed by a combination of chain-cut and peripheral-cut ions. Molecular ions formed during ESI can easily be converted to peripheral-cut ions in the MS/MS process. Similarly, chain-cut ions can also be readily converted to chain-plus-peripheral-cut ions (Figure 5).

Typical chain-cut ions for LMs in MS/MS are formed by α-cleavage of the carbon-carbon bonds connecting to the
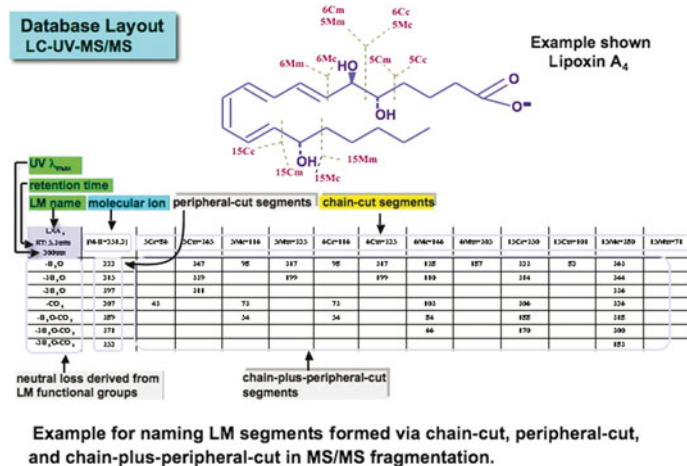
Figure 5. Liquid chromatography-ultra violet and tandem mass spectrometry (LC-UV-MS/MS) database layout: example for naming lipid mediators (LM) segments. In this case, the example shown is lipoxin A_4, formed via chain-cut, peripheral-cut, and chain-plus-peripheral-cut for interpretation of tandem mass spectrometry (MS/MS) fragmentation.

carbon with a functional group directly attached.[4,9,13,19,20] LMs readily undergo α-cleavage.[13] We proposed the nomenclatures illustrated in the LXA_4 structure presented in Figure 5 to systematically name the segments formed via chain-cut and chain-plus-peripheral-cut without concern for hydrogen shift occurring during MS analysis of PUFA-derived products. Each of these LMs derived from PUFA has a carboxyl terminus and a methyl terminus. An Arabic number was used to designate the position of the functional group on the LM carbon chain where the cleavage occurs. The upper-case letter right after the number indicates the side of the functional group on which the cleavage occurs: C is for cleavage on the carboxyl side of the functional group, and M is for cleavage on the methyl side of the functional group. Each cleavage can directly generate 2 segments. The lower-case letter that follows indicates the side of the cleavage on which the segment forms: c is for a segment formed on the carboxyl side of the cleavage, and m is for a segment formed on the methyl side of the cleavage. Segments formed through β-cleavage or γ-cleavage toward the functional group are named by adding β or γ between the upper-case and lower-case letters. Because 3 hydroxy groups of LXA_4 are located at C_5, C_6, and C_{15} of the 20-carbon linear chain, α-cleavages can occur on the bonds at C_4-C_5, C_5-C_6, C_6-C_7, C_{14}-C_{15}, and C_{15}-C_{16} to generate 10 chain-cut segments (Figure 5). All the possible chain-cut, peripheral-cut, and chain-plus-peripheral-cut segments for LXA_4 are indicated in Figure 5.

An MS/MS ion detected from LM samples in negative-ion mode generally is formed from a specific segment with the addition or subtraction of hydrogen(s) caused by hydrogen shift during the cleavage. The charge (z) of the LM negative ion is usually equal to 1; therefore, the mass-to-charge ratio

(m/z) of an LM ion is usually equals to its mass (m). Previous reports[13,18,19] and our past results[4,6-9,20] have demonstrated that the MS/MS fragmentation observes the empirical rules on the addition or subtraction of hydrogen(s) for the chain-cut segments to form the chain-cut MS/MS ions.

- For the segment Cc, the detected MS/MS ions are Cc and Cc + H.

- For the segment Cm, the detected MS/MS ions are Cm, Cm ± H, and Cm ± 2H.

- For the segment Mc, the detected MS/MS ions are Mc and Mc − H.

- For the segment Mm, the detected MS/MS ions are Mm, Mm ± H, and Mm ± 2H.

These rules were used to identify the segments for instrument-detected MS/MS ions. The interpreted ions, such as M − H − H_2O, Cc, Cc + H, or Mc − H, identified as the MS/MS ions detected in the mass spectrometer, are called virtual ions. One detected MS/MS ion can be interpreted as one or several virtual ions. Through loss of H_2O, CO_2, NH_3, and/or amino acids, the chain-cut ions can form chain-plus-peripheral-cut ions. For the chain-cut and chain-plus-peripheral-cut ions in the present report, we focused on those formed by α-cleavages. Detected MS/MS ions that are uninterpretable via the general rules noted above and neutral loss are taken as unidentified ions.

Modification of MS/MS Ion Intensities According to Identities

In nature, isotope ^{13}C is 1.1% of elemental carbon. If the intensity of an ion with mass M (ion charge z is 1) containing only carbons, hydrogens, and oxygen(s) is 100, the contribution of ^{13}C to the intensity of the ion with mass (M + 1) (the ion with mass 1 unit higher) is statistically equal to $100 \times 1.1\% \times$ number of carbons in the ion M (see McLafferty and Turecek).[25] The contribution of ^{13}C to the ion (M + 2) is much less than $100 \times 1.1\% \times$ carbon number. Thus, the ^{13}C contribution of ion M to the intensities of ions (M + 1) and (M + 2) was subtracted in the computation of the matching score for COCAD and theoretical algorithms. If ion M could not be identified, the carbon number in the ion (M + 1) or (M + 2) is used because M, (M + 1), and (M + 2) generally have the same carbon number.

Chain-cut ions are most informative and could be diagnostic for determining specific LM structures such as the position of functional groups and double bonds. Generally, there are more chain-plus-peripheral-cut ions than chain-cut ions because the former are derived from the latter by one or several neutral losses. It is likely that some chain-plus-peripheral-cut ions have the same m/z even though they originate by different mechanisms and represent different structural features. Therefore, chain-cut ions are more

specific than chain-plus-peripheral-cut ions for defining the LM structure. Peripheral-cut ions in MS/MS spectra are similar among LM isomers and, therefore, were not specific enough for differentiation of individual LM isomers.

According to the general fragmentation rule noted above, the nth MS/MS peak can be identified as one or several chain-cut (*C*) ions, peripheral-cut (*P*) ions, and/or chain-plus-peripheral-cut (*CP*) ions. The weighted intensity ^yI_n of each identified ion is as follows:

$$y_{I_n} = I_n' \div \left({}_n^C M + {}_n^{CP} M + {}_n^P M \times \rho \right) \times {}^y W \qquad (1)$$

where *y* is the MS/MS ion type identified as *C*, *P*, or *CP*; I_n' is the relative intensity of the nth peak in the MS/MS spectrum; ${}_n^C M$ is the number of chain-cut ions identified for the nth MS/MS peak; ${}_n^{CP} M$ is the number of chain-plus-peripheral-cut ions identified for the nth MS/MS peak; ${}_n^P M$ is the number of peripheral-cut ions identified for the nth MS/MS peak; and ^yW is the weight measuring the importance of the identified ion to determine the LM structure. It is 10 as ^CW and 1 as ^{CP}W or ^PW (for peripheral-cut ions). The fingerprint features of chain-cut ions are used to define LM structure by multiplying their intensities by 10, which was determined to be the best among the tested values of 2, 10, 20, and 100. Weighted MS/MS ion intensities are used for COCAD and the theoretical system described below. ρ represents the contribution of peripheral-cut ions to I_n' ($\rho = 3$ for peripheral-cut ions formed via loss of one CO_2 from each molecular ion, $\rho = 10$ for peripheral-cut ions formed via loss of one H_2O from each molecular ion, and $\rho = 1$ for other peripheral-cut ions formed via multiple loss of CO_2 and/or H_2O from each molecular ion). The assignment of ρ values is arbitrary and based on the observation of relative intensities of peripheral-cut ions in MS/MS spectra of LMs.

COCAD Contrast Angle

COCAD used a contrast-angle algorithm to match an MS/MS spectrum between sample and standards. For this approach, the contrast angle is calculated as follows:

$$C_v = \sum_{n=1}^{N} \left({}_n^C B_v \times C_{I_n} \right) \qquad (2)$$

$$CP_v = \sum_{n=1}^{N} \left({}_n^{CP} B_v \times CP_{I_n} \right) \qquad (3)$$

$$P_v = \sum_{n=1}^{N} \left({}_n^P B_v \times P_{I_n} \right) \qquad (4)$$

$$D_C(D_{CP}, \text{or } D_P) = \frac{\sum_{v=1}^{V} U_v S_v}{\sqrt{\sum_{v=1}^{V} U_v^2 \sum_{v=1}^{V} S_v^2}} \qquad (5)$$

U_v is equal to C_v, CP_v, or P_v for unknown spectrum to be identified

S_v is equal to C_v, CP_v, or P_v for standard spectrum

$$\text{COCAD contrast angle} = Cos^{-1}[(10 \times D_C + D_P + D_{CP}) \div (11 + w_{CP})] \qquad (6)$$

where v is the vth virtual ion; V is the total number for one type of virtual ion formed via chain-cut, chain-plus-peripheral-cut, or peripheral-cut for a specific LM; ${}_n^C B_v$ is equal to 1 if the nth MS/MS peak can be identified as the vth virtual ion formed via chain-cut, or equal to 0 if not; ${}_n^{CP} B_v$ or ${}_n^P B_v$ has a similar meaning but for ions formed via chain-plus-peripheral-cut or peripheral-cut; *N* is the total number of peaks in the MS/MS spectrum; D_C is the dot product between the virtual vectors of *U* (unknown sample) and *S* (standard) formed via chain-cut; and D_{CP} or D_P is the dot product for chain-plus-peripheral-cut or peripheral-cut ions, respectively. D_C, D_{CP}, or D_P in Equation 5 represents the similarity of ions formed via chain-cut, chain-plus-peripheral-cut, or peripheral-cut, between an unknown spectrum and a standard spectrum, none of which had a value greater than 1. The vth virtual ion is not used for the calculation of the corresponding D_C, D_{CP}, or D_P if either U_v or S_v is 0. If every C_v, CP_v, or P_v within the vectors is 0, then D_C, D_{CP}, or D_P is assigned the value 0.

The COCAD contrast angle in Equation 6 indicates how well the spectrum of the sample matches the standard: if it is 0°, the 2 spectra match exactly; if it is 90°, the 2 spectra do not match at all; the smaller the contrast angle between 0° and 90°, the better the match.[16,26] The value is integrated and normalized from dot products D_C, D_{CP}, or D_P (Equation 6). The numeric coefficient 10 in Equation 6 was found to be the best value (2, 20, and 100 were also tested) that emphasizes the fingerprinting feature of chain-cut ions because chain-cut ions are more important for determining the LM structure than are other types of ions. To normalize $[(10 \times D_C + D_{CP} + D_P) \div (11 + \omega_{CP})]$ in Equation 6 to be no more than 1, 11 was used in the denominator of Equation 6, and ω_{CP} is equal to 1 if at least one MS/MS ion is identified as a chain-plus-peripheral-cut virtual ion or equal to 0 if no such ion is identified. No chain-plus-peripheral-cut ion is identified in a few LM standard spectra. Therefore, ω_{CP} is introduced in Equation 6 to normalize the COCAD contrast angle to 0 when matching these types of spectra against themselves. Unidentified ions were excluded for matching in Equations 2 to 6.

According to the general rules, for monohydroxy-containing LMs, the vth chain-cut ion can be Cc, Cc + 1, Cm − 2, Cm − 1, Cm, Cm + 1, Cm + 2, Mc − 1, Mc, Mm − 2, Mm − 1, Mm, Mm + 1, or Mm + 2. The vth chain-plus-peripheral-cut ion is Cc − CO_2, Cc − CO_2 + 1, Cm − H_2O − 2, Cm −

$H_2O - 1$, $Cm - H_2O$, $Cm - H_2O + 1$, $Cm - H_2O + 2$, $Mc - H_2O - 1$, $Mc - H_2O$, $Mc - CO_2 - 1$, $Mc - CO_2$, $Mc - H_2O - CO_2 - 1$, or $Mc - H_2O - CO_2$. The νth peripheral-cut ion is $M - H - CO_2$, $M - H - H_2O$, or $M - H - H_2O - CO_2$. For LMs having multiple functional groups, V is accordingly greater.

Integrating MS/MS Spectra With UV Spectra and Chromatograms in COCAD to Identify LMs

COCAD incorporates the LC-UV-MS/MS chromatograms and spectra measured from standard LMs and the segments formed by cleavage illustrated in Figure 5. The features of UV spectra and chromatograms are represented with the UV λ_{max} and CRTs, respectively. The search of COCAD was conducted stepwise, as depicted in the logic diagram in Figure 3, from UV λ_{max}, to MS/MS spectra, and then to CRTs. Using COCAD, we identified LXA$_4$ in murine spleen stimulated during exposure to *T* (Toxoplasma) *gondii* (Figure 6A and 6B). The search was narrowed down to the sub-database with UV λ_{max} 301 nm (middle inset) and molecular ion *m/z* 351, which were detected for the unknown peak II in the chromatogram (*m/z* 251 of MS/MS 351) for the stimulated spleen sample. The CRT (5.2 minutes) of peak II was then matched against the candidates with the highest MS/MS match score (Figure 6A left inset). For comparison, searching was also conducted with the system developed via MassFrontier (Figure 6C). Both demonstrated that LXA$_4$ was the best match for the unknown peak II shown in Figure 6A. However, COCAD and MassFrontier could not be used alone to identify the structures of unknowns without LC-UV-MS/MS chromatograms and spectra obtained for authentic and/or synthetic standards.

THEORETICAL DATABASE AND SEARCH ALGORITHM FOR NOVEL LM IDENTIFICATION

Theoretical databases consist of the segments (as illustrated in Figure 5), the UV λ_{max}, and CRTs predicted for potentially novel LMs. Searching against a theoretical database is

Figure 6. COCAD-based identification of LXA$_4$ in murine spleens. Mice were exposed to *T* (Toxoplasma) *gondii* as in Aliberti et al.[24] COCAD used was developed in Lu et al[3] (representative, n = 3). (A) Identification, interpretation, and annotation of anions in MS/MS (at *m/z* 351) spectra. The MS/MS scan conditions were parent ion, *m/z* 351; isolation width, 1.5; normalized collision energy, 35%; activation time, 30 ms; and scan of MS/MS ions, *m/z* 95 to 355. The insets are chromatogram (at *m/z* 251 of MS/MS 351, left), UV spectrum (middle), and proposed MS/MS segments on LXA$_4$ (right). The chromatogram at *m/z* 251 of MS/MS 351 was the intensity temporary profile or extracted chromatogram for ion *m/z* 251 in the MS/MS spectrum of parent ion *m/z* 351 generated in ESI (electrospray ionization). (B) Report shows LXA$_4$ identified as the best match for the LC-UV-MS/MS (liquid chromatography-ultra violet and tandem mass spectrometry) results in the COCAD system (with highest match score). (C) LXA$_4$ was also identified by searching the database constructed by MassFrontier. (MS/MS, tandem mass spectrometry; *m/z*, mass to charge ratio; and COCAD, cognoscitive-contrast-angle algorithm and databases.)

also performed stepwise as described in Figure 3, from UV $\lambda_{\max}$, to MS/MS spectra, and then to CRTs.

Equation 7 is the matching score for an unknown MS/MS spectrum compared with the virtual spectrum based on the segments and fragmentation rule noted above:

$$\left\{ \sum_{f=1}^{F} \left[\sum_{n=1}^{N} \left(C_{I_n} \times {}_f^C M_n \right) \times \left({}^f T_C \div {}^f A_C \right)^{0.5} \right] \right. $$
$$+ \sum_{f=1}^{F} \left[\sum_{n=1}^{N} \left(CP_{I_n} \times {}_f^{CP} M_n \right) \times \left({}^f T_{CP} \times {}^f A_{CP} \right)^{0.5} \right] \tag{7}$$
$$\left. + \sum_{n=1}^{N} \left[P_{I_n} \times P_{M_n} \times (T^P \div A^P)^{0.5} \right] \right\} \div \sum_{n=1}^{N} \left(C_{I_n} + CP_{I_n} + P_{I_n} \right)$$

The matching score in Equation 7 summates the weighted intensities of all the identified MS/MS peaks in the spectrum acquired from the sample. The numerator of this formula is composed of 3 parts:

$$\sum_{f=1}^{F} \left[\sum_{n=1}^{N} \left(C_{I_n} \times {}_f^C M_n \right) \times \left({}^f T_C \div {}^f A_C \right)^{0.5} \right] \tag{8}$$

summating the weighted intensities of MS/MS peaks identified as chain-cut ions;

$$\sum_{f=1}^{F} \left[\sum_{n=1}^{N} \left(CP_{I_n} \times {}_f^{CP} M_n \right) \times \left({}^f T_{CP} \div {}^f A_{CP} \right)^{0.5} \right] \tag{9}$$

summating the weighted intensities of MS/MS peaks identified as chain-plus-peripheral-cut ions; and

$$\sum_{n=1}^{N} \left[P_{I_n} \times P_{M_n} \times (T_P \div A_P)^{0.5} \right] \tag{10}$$

summating the weighted intensities of MS/MS peaks identified as peripheral-cut ions. ${}_f^C M_n$ is the total number of chain-cut ions via α-cleavage formed from the fth functional group and matched to the nth MS/MS peak. F is the total number of functional groups in 1 LM, and f is counted from the carboxyl terminus of LM. For example, f is 1 for the 5-hydroxy, 2 for the 6-hydroxy, and 3 for the 15S-hydroxy group present in LXA$_4$. F for LXA$_4$ is 3 (Figure 5). $\left(\sum_{n=1}^{N} \left({}^C_f I_n \times {}_f^C M_n \right) \right)$ summates the weighted intensities of MS/MS peaks identified as chain-cut ions formed from the fth functional group via α-cleavage. The smallest MS/MS ion detectable in ion-trap tandem MS is generally $\sim m/z$ 95 for LMs with a molecular ion of $\sim$400 d.[27] To compensate for the bias caused by the inability to detect an MS/MS ion of m/z less than 95, factors $({}^f T_C \div {}^f A_C)^{0.5}$, $({}^f T_{CP} \div {}^f A_{CP})^{0.5}$ and $(T_P \div A_P)^{0.5}$ are used in Equation 7. ${}^f T_C$ (or ${}^f T_{CP}$) is the total number of chain-cut (or chain-plus-peripheral-cut) ions formed from the fth functional group via α-cleavage. T_P is the total number of peripheral-cut ions formed from 1 LM. ${}^f A_C$ (${}^f A_{CP}$, or A_P) is the fraction of ${}^f T_C$ (${}^f T_{CP}$ or T_P) representing the ions within the MS/MS detecting range (m/z from 95 to the m/z of molecular ion). 20-HETE is a typical example. The ions formed from

the segment 20Cm and 20Cm – H$_2$O of 20-HETE are m/z 31 and 13 according to our general fragmentation rules noted above, which are too small to be detected in ion-trap MS/MS. Consequently, without the use of factors $({}^f T_C \div {}^f A_C)^{0.5}$ and $({}^f T_{CP} \div {}^f A_{CP})^{0.5}$, 20-HETE could have a lower matching score than other HETEs even though the MS/MS spectrum is that of 20-HETE. $\left(\sum_{n=1}^{N} \left(C_{I_n} + CP_{I_n} + P_{I_n} \right) \right)$ is used in Equation 7 for normalization to eliminate the impact on the matching scores of the total peak intensities in MS/MS spectra.

Unknown MS/MS spectra were assigned to the LM and/or potentially novel LM that had the highest matching score in addition to having the predicted UV spectral and chromatographic features (eg, $\lambda_{\max}$ and CRTs). This theoretical system was used successfully to identify 15S-HETE in murine spleen (Figure 3).[3] Peak III displayed at CRT 20.4 minutes on the chromatogram (at m/z 219 of MS/MS 319) had a UV $\lambda_{\max}$ of 235 nm. Therefore, the search on the theoretical system was narrowed down to the subdatabase with molecular ion m/z 319, UV $\lambda_{\max}$ 235 nm, and CRT 21 minutes. In this example, 15-HETE gave the highest matching score among all compounds in the subdatabase.[3] The MS/MS peaks identified were annotated with the ion interpretation that also shows a fragmentation mechanism. Segments of 15-HETE that matched the MS/MS peaks according to the fragmentation rules noted above are italicized in red, in Panel B of Figure 6.[3] For comparison, MassFrontier was also used to identify peak III, which also identified it as 15-HETE.

We used LC-UV-MS/MS chromatograms and spectra acquired from murine tissue and organ extracts spiked with >34 well-known LMs and related compounds for the evaluation. For every known compound added (ie, spiked) in all samples, the search of its LC-UV-MS/MS through a database gives a "hit list" showing what compound matches best. The best match has the highest matching score using the MassFrontier or theoretical database, and the smallest contrast angle using COCAD. Hence, the best match is either correct or incorrect. The mean and SE of percent correct for best match indicated the performance of each database and algorithm. Generally, COCAD offered the greatest percent correct,[3] which was considered reasonable because COCAD takes into account both MS/MS ion intensities and identities measured from authentic eicosanoid standards and unknowns. The percent correct from the theoretical system is comparable to that of MassFrontier.[3]

Our test results demonstrated that it was not necessary to use all the MS/MS ions to identify an LM or other compounds.[3] Also, in some cases it is neither simple nor cost-efficient to identify all MS/MS ions. Rigorous identification can be performed using isotope labeling and derivatization, which may not be feasible or realistic to apply to routine analyses of biologically relevant samples. Thus, we can identify an LM with precision using one to several chain-cut

ions per functional group along with peripheral-cut ions and chain-plus-peripheral-cut ions following the MS/MS fragmentation rules. For example, we use at least 4 ions for monohydroxy-containing eicosanoids, 6 ions for dihydroxy-containing eicosanoids, and 8 ions for trihydroxy-containing eicosanoids. The Eight Peak Index of Mass Spectra database is used for manual identification of compounds.[28] For different amounts of LMs added to the samples (1.0, 2.5, and 5.0 ng), the percent identified correctly was not significantly different. Based on the test experiments using the theoretical database and algorithm, the average matching score for correct best match is 2.02 with a standard error of 0.71 (n = 212). Therefore, the threshold score for a 95% confidence interval of matching score for correct best match is 2.02 – (1.96 × 0.71) = 0.62.

The databases and search algorithms were developed on the basis of LC-UV-ion trap MS/MS data of LMs. The ion intensity patterns of MS/MS spectra generated from an ESI-triple-quadrupole mass spectrometer are quite similar to ESI-ion trap MS because the collision energy for both types of instruments is in the low energy region (a few to 100 eV, laboratory kinetic energy of ions).[7,13,24,29] Therefore, the constants and algorithms reviewed here from Lu et al[3] may fit the CID spectra from triple-quadrupole MS/MS without much modification. For high–collision energy (several 10^2 to ~10^3 eV) CID spectra generated via sector or TOF/TOF (time of flight/time of flight) analyzer, the relative intensity patterns are quite different in comparison with the low energy ones, although many ions occurred for both energy situations[7,13,19,24,29]; for example, the peripheral-cut ions are less abundant than the chain-cut ions. For ion-trap and triple-quadrupole MS/MS, peripheral-cut ions are more abundant than chain-cut ions. Our constants and algorithms give chain-cut ions more weight than peripheral-cut ions because chain-cut ions are more important to defining LM structures. Therefore, they may still fit high–collision energy CID spectra. Nevertheless, the constants and algorithms should be thoroughly tested and modified accordingly so that they can be validated for use with other instruments that may give fragmentation patterns of different intensities than the instruments used herein.

The CRTs used in this set of experiments were obtained using specified chromatographic conditions (for a column of 100 mm or 150 mm length) and because several fundamental issues were our initial focus. Hence, the databases and algorithms were programmed so that the new LC-UV-MS/MS data including other chromatographic conditions can be easily entered and used in the databases.

This full cycle of events defines mediator-based lipidomics because it is important to establish both the structure and functional relationships of bioactive molecules in addition to their cataloging and mapping of architectural components of biolipidomics. With this new informatics and lipidomics-based approach that combined LC-PDA (photodiode array)-MS/MS (Figures 2 and 3), a novel array of endogenous LMs were identified[4,9] during the multicellular events that occur as inflammation resolves. The novel biosynthetic pathways uncovered use omega-3 fatty acids, eicosapentaenoic acid, and docosahexaenoic acid as precursors to new families of protective molecules, termed resolvins and protectins (Figures 1B and 7). These include resolvin E (18*R* series from EPA, eicosapentaenoic acid) and 17 series resolvin D series from DHA (docosahexaenoic acid).[20] In humans, the vasculature, in particular endothelial cells during cross-talk with leukocytes, generate these products via transcellular biosynthesis pathways.[4] In this novel cell-cell interaction, endothelial cells generate the first biochemical step and then pass this intermediate 18*R*-HEPE to leukocytes, which transform this into a potent molecule termed resolvin E1 (RvE1) (Figure 8). RvE1 is ~1000 times more potent than
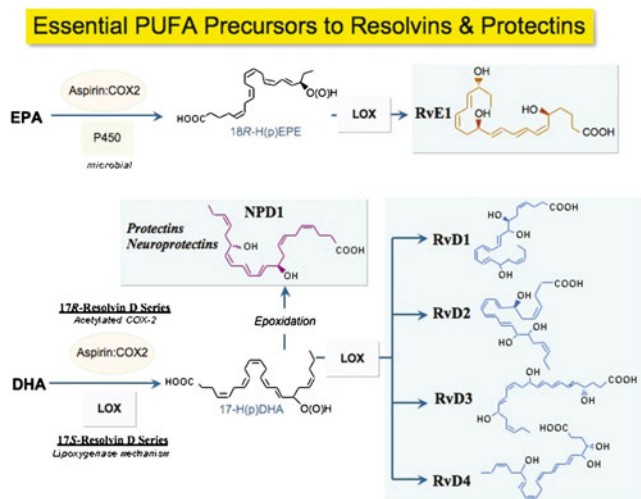

Figure 7. Formation of resolvin E1 derived from EPA (eicosapentaenoic acid), resolvin D1, protectins, and neuroprotectin D1 and from DHA (docosahexaenoic acid).
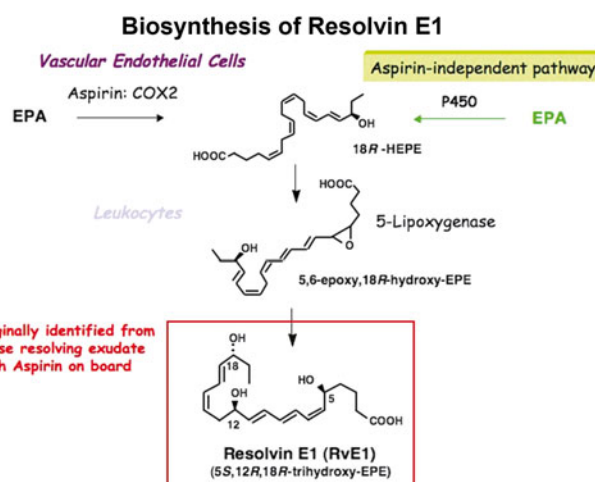

Figure 8. Biosynthesis pathway of resolvin E1.

native EPA as a downregulator of neutrophils and stops their migration into inflammatory loci.[4,9,12]

DHA, which is enriched in neural systems,[30] is also released and transformed into potent bioactive molecules denoted 10R,17S docosatriene or neuroprotectin D1[31] and resolvins of the D series (Figure 7). The human brain, synapses, and retina are rich in DHA, a major omega-3 fatty acid. Deficiencies in DHA are associated with altered neural functions, cancer, and inflammation in experimental animals.[32] Employing our mediator-based lipidomics approach, we found that on activation, neural systems release DHA to produce neuroprotectin D1, which in addition to stopping leukocyte-mediated tissue damage in stroke also maintains retinal integrity.[33] Of interest, fish rich in DHA such as rainbow trout generate NPD1 and resolvins of the D series (Figure 9). These findings raise the question of their role in the biological systems of fish and suggest that lipid mediators are highly conserved structures in the course of evolution.[34]

CONCLUSIONS AND FUTURE CHALLENGES FOR LM LIPIDOMICS

At this juncture, we can begin to appreciate the temporal differences as well as spatial components within sites of inflammation that are responsible for generating specific local acting lipid-derived mediators. The immediate future will bring forth the mapping of local biochemical mediators and reveal the potential impact of drugs, diet, and stress—that is, hypoxia and ischemia reperfusion within these bionetworks. Moreover, these results will enable us to further appreciate the fact that what matters in health and disease is not the size of the peak but the bioaction or functional impact within organ systems. Transient, seemingly small, quantitatively fleeting members of LM pathways and their temporal relationship change extensively during a physiologic and/or pathophysiologic response. These changes in magnitude of LMs and their interrelationships within a given profile of autacoids/local mediators are part of a complex network of events that typifies the decoding power of LM-based informatics-lipidomics.

The main obstacle presently for this area is to devise meaningful ways to visually present the large amounts of data obtained from biological process mapping using this and related MS and informatics approaches to the study of lipid-derived mediators. Standardization of data acquisition, instrumentation and instrument settings, synthetic authentic and LMs, and spectral libraries is a critical part of sharing and unifying the information to achieve an understanding of
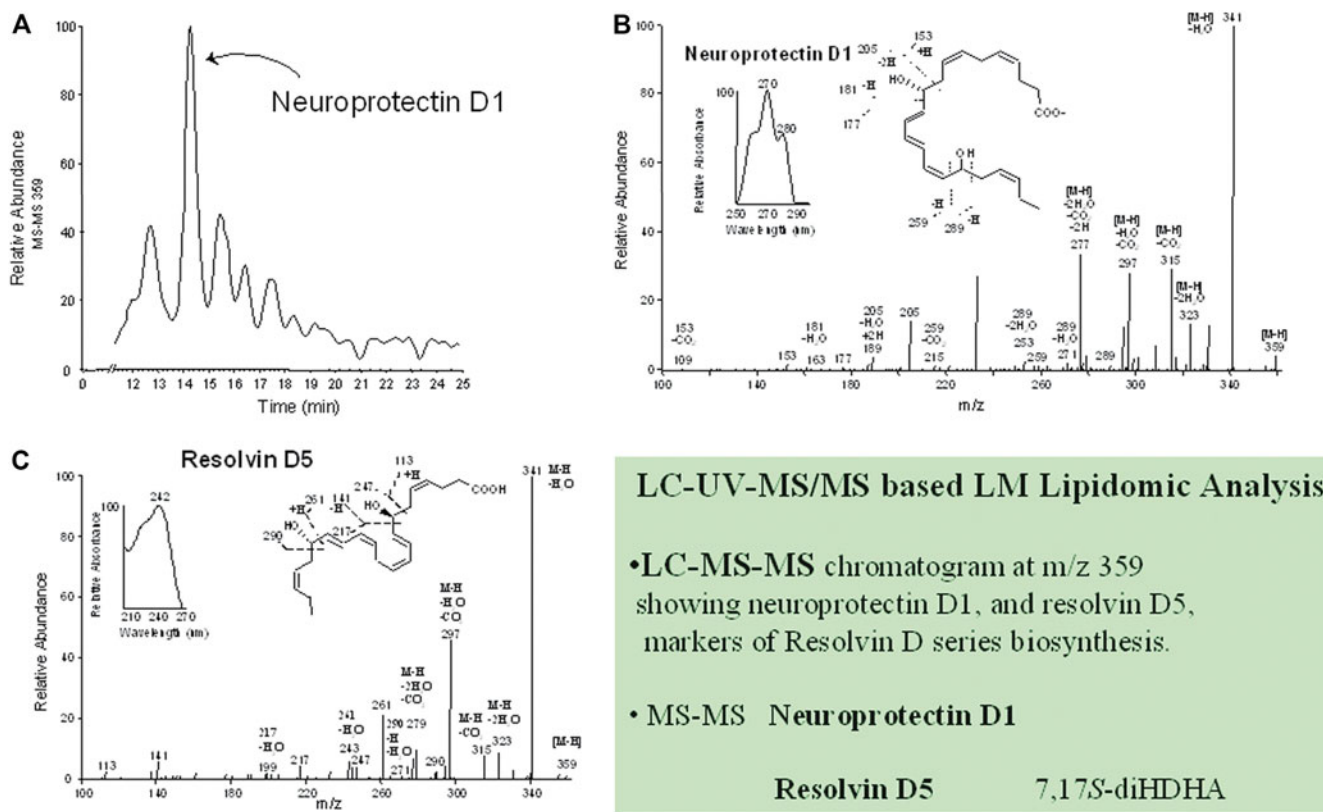

Figure 9. Trout brain cells generate neuroprotectin D1 and resolvin D5. The DHA (docosahexaenoic acid)-derived products were identified by LC-UV-MS/MS (liquid chromatography-ultra violet and tandem mass spectrometry)-based lipidomic analysis. (A) LC-MS/MS, liquid chromatography-tandem mass spectrometry, (at *m/z*, ion of mass/charge ratio, 359) chromatogram showing 2 10,17*S*-docosatrienes, neuroprotectin D1, and resolvin D5 (7,17*S*-diHDHA), which are markers of resolvin D series biosynthesis. (B) A representative MS/MS spectrum of 10,17*S*-docosatrienes in Panel A. (C) MS/MS spectrum of resolvin D5.

the vast complexities in the biological processes of interest. Once these challenges are met, we can standardize the approach and methods to obtain results from individuals in health as well as specific disease states or even during a common cold. For example, it should soon be possible for a clinician to routinely screen patients to determine whether their daily dose of aspirin is effective for them. Moreover, the modest steps taken today shall enable large-scale population studies of LM profiles, their local levels in situ, and their serum PUFA precursor levels. Also, for example, local LMs and their relationships to an individual's diet, genomic makeup, disease status, and general host defense status could be analyzed. Given the advances in nanotechnologies and likely increases in sensitivity of mass spectrometers, it should be possible to develop personalized units to continuously monitor an individual's profile of proinflammatory LMs as well as those involved in resolution of inflammation. Also, it should be possible for a clinician to monitor individuals' metabolic interaction with specific microbes and the individuals' own metabolome within, for example, the oral cavity. Considering these possibilities raises the question of whether it will be possible to correct and/or compensate for individual alteration in LM pathways to improve health, modulate disease status, and prevent disease via enhancing host defense mechanisms with these and/or related molecules. Addressing questions along these lines are some of the future challenges for the exciting new field of LM informatics-lipidomics and metabolomics.

ACKNOWLEDGMENTS

REFERENCES

1. Samuelsson B, Dahlén SE, Lindgren JÅ, Rouzer CA, Serhan CN. Leukotrienes and lipoxins: structures, biosynthesis, and biological effects. *Science*. 1987;237:1171-1176.

2. Bergström S. The prostaglandins: from the laboratory to the clinic. In: The Nobel Foundation, ed. *Les Prix Nobel: Nobel Prizes, Presentations, Biographies and Lectures.* Stockholm, Sweden: Almqvist & Wiksell; 1982:129-148.

3. Lu Y, Hong S, Tjonahen E, Serhan CN. Mediator-lipidomics: databases and search algorithms for PUFA-derived mediators. *J Lipid Res*. 2005;46:790-802.

4. Serhan CN, Clish CB, Brannon J, Colgan SP, Chiang N, Gronert K. Novel functional sets of lipid-derived mediators with antiinflammatory actions generated from omega-3 fatty acids via cyclooxygenase 2-nonsteroidal antiinflammatory drugs and transcellular processing. *J Exp Med*. 2000;192:1197-1204.

5. Hannun YA, Obeid LM. The ceramide-centric universe of lipid-mediated cell regulation: stress encounters of the lipid kind. *J Biol Chem*. 2002;277:25847-25850.

6. Gronert K, Kantarci A, Levy BD, et al. A molecular defect in intracellular lipid signaling in human neutrophils in localized aggressive periodontal tissue damage. *J Immunol*. 2004;172:1856-1861.

7. Serhan CN, Jain A, Marleau S, et al. Reduced inflammation and tissue damage in transgenic rabbits overexpressing 15-lipoxygenase and endogenous anti-inflammatory lipid mediators. *J Immunol*. 2003;171:6856-6865.

8. Levy BD, Clish CB, Schmidt B, Gronert K, Serhan CN. Lipid mediator class switching during acute inflammation: signals in resolution. *Nat Immunol*. 2001;2:612-619.

9. Serhan CN, Hong S, Gronert K, et al. Resolvins: a family of bioactive products of omega-3 fatty acid transformation circuits initiated by aspirin treatment that counter pro-inflammation signals. *J Exp Med*. 2002;196:1025-1037.

10. Calder PC. Polyunsaturated fatty acids, inflammation, and immunity. *Lipids*. 2001;36:1007-1024.

11. Serhan CN. Mediator lipidomics. *Prostaglandins Other Lipid Mediat*. 2005;77:4-14.

12. Serhan CN, Gotlinger K, Hong S, Arita M. Resolvins, docosatrienes, and neuroprotectins, novel omega-3-derived mediators, and their aspirin-triggered endogenous epimers: an overview of their protective roles in catabasis. *Prostaglandins Other Lipid Mediat*. 2004;73:155-172.

13. Murphy RC, Fiedler J, Hevko J. Analysis of nonvolatile lipids by mass spectrometry. *Chem Rev*. 2001;101:479-526.

14. Ausloos P, Clifton CL, Lias SG, et al. The critical evaluation of a comprehensive mass spectral library. *J Am Soc Mass Spectrom*. 1999;10:287-299.

15. Stein SE. Chemical substructure identification by mass spectral library searching. *J Am Soc Mass Spectrom*. 1995;6:644-655.

16. Stein SE, Scott DR. Optimization and testing of mass spectral library search algorithms for compound identification. *J Am Soc Mass Spectrom*. 1994;5:859-866.

17. Mallard GW, Reed J. *Automated Mass Spectral Deconvolution & Identification Systems.* Gaithersburg, MDUS Department of Commerce—Technology Administration, National Institutes of Standards and Technology Standard Reference Data Program: 1997.

18. Chiang N, Takano T, Clish CB, Petasis NA, Tai H-H, Serhan CN. Aspirin-triggered 15-epi-lipoxin A_4 (ATL) generation by human leukocytes and murine peritonitis exudates: development of a specific 15-epi-LXA_4 ELISA. *J Pharmacol Exp Ther*. 1998;287:779-790.

19. Griffiths WJ, Yang Y, Sjövall J, Lindgren JÅ. Electrospray/collision-induced dissociation mass spectrometry of mono-, di- and tri-hydroxylated lipoxygenase products, including leukotrienes of the B-series and lipoxins. *Rapid Commun Mass Spectrom*. 1996;10:183-196.

20. Hong S, Gronert K, Devchand P, Moussignac R-L, Serhan CN. Novel docosatrienes and 17S-resolvins generated from docosahexaenoic acid in murine brain, human blood and glial cells: autacoids in anti-inflammation. *J Biol Chem*. 2003;278:14677-14687.

21. Wenk MR, Lucast L, Paolo GD, et al. Phosphoinositide profiling in complex lipid mixtures using electrospray ionization mass spectrometry. *Nat Biotechnol*. 2003;21:813-817.

22. Serhan CN. On the relationship between leukotriene and lipoxin production by human neutrophils: evidence for differential metabolism of 15-HETE and 5-HETE. *Biochim Biophys Acta*. 1989;1004:158-168.

23. Kiss L, Bieniek E, Weissmann N, et al. Simultaneous analysis of 4- and 5-series lipoxygenase and cytochrome P450 products from different biological sources by reversed-phase high-performance liquid chromatographic technique. *Anal Biochem*. 1998;261:16-28.

24. Aliberti J, Hieny S, Reis e Sousa C, Serhan CN, Sher A. Lipoxin-mediated inhibition of IL-12 production by DCs: a mechanism for regulation of microbial immunity. *Nat Immunol*. 2002;3:76-82.

25. McLafferty FW, Turecek F. Elemental composition. In: Imfeld I, Kelly A, eds. *Interpretation of Mass Spectra*. 4th ed. Mill Valley, CA: University Science Books; 1993:19-34.

26. Wan KX, Vidavsky I, Gross ML. Comparing similar spectra: from similarity index to spectral contrast angle. *J Am Soc Mass Spectrom*. 2002;13:85-88.

27. User Manual LCQ™. San Jose, CA: Finnigan MAT; 1996.

28. McLafferty FW, Stauffer DA, Loh Y, Wesdemiotis C. Unknown identification using reference mass spectra: quality evaluation of databases. *J Am Soc Mass Spectrom*. 1999;10: 1229-1240.

29. Wheelan PJ, Zirrolli JA, Murphy RC. Electrospray ionization and low energy tandem mass spectrometry of polyhydroxy unsaturated fatty acids. *J Am Soc Mass Spectrom*. 1996;7:140-149.

30. Salem N Jr, Litman B, Kim H-Y, Gawrisch K. Mechanisms of action of docosahexaenoic acid in the nervous system. *Lipids*. 2001;36:945-959.

31. Serhan CN, Gotlinger K, Hong S, et al. Anti-inflammatory actions of neuroprotectin D1/protectin D1 and its natural stereoisomers: assignments of dihydroxy-containing docosatrienes. *J Immunol*. 2006;176:1848-1859.

32. Burr GO, Burr MM. A new deficiency disease produced by the rigid exclusion of fat from the diet. *J Biol Chem*. 1929;82:345-367.

33. Mukherjee PK, Marcheselli VL, Serhan CN, Bazan NG. Neuroprotectin D1: a docosahexaenoic acid-derived docosatriene protects human retinal pigment epithelial cells from oxidative stress. *Proc Natl Acad Sci USA*. 2004;101:8491-8496.

34. Hong S, Tjonahen E, Morgan EL, Yu L, Serhan CN, Rowley AF. Rainbow trout (*Oncorhynchus mykiss*) brain cells biosynthesize novel docosahexaenoic acid-derived resolvins and protectins—mediator lipidomic analysis. *Prostaglandins Other Lipid Mediat*. 2005;78:107-116.